IEEE Access
Multidisciplinary | Rapid Review | Open Access Journal

Received March 29, 2019, accepted April 25, 2019, date of publication May 1, 2019, date of current version May 13, 2019.

Digital Object Identifier 10.1109/ACCESS.2019.2914124

Design and Analysis of a Square-Shaped Continuum Robot With Better Grasping Ability

LONG LI[1,2], TAO JIN[1,2], YINGZHONG TIAN[1,2], FEI YANG[3], AND FENGFENG XI[1,2,4]

[1]School of Mechatronic Engineering and Automation, Shanghai University, Shanghai 200072, China
[2]Shanghai Key Laboratory of Intelligent Manufacturing and Robotics, Shanghai 200444, China
[3]School of Mechatronics Engineering, Harbin Institute of Technology, Harbin 150001, China
[4]Department of Mechanical, Aerospace, and Industrial Engineering, Ryerson University, Toronto, ON M5B 2K3, Canada

Corresponding author: Yingzhong Tian (troytian@shu.edu.cn)

This work was supported in part by the National Science Foundation for Young Scientists of China under Grant 51705098, in part by the Special Plan of Major Scientific Instruments and Equipment of the State under Grant 2018YFF01013101, in part by the IIOT Innovation and Development Special Foundation of Shanghai under Grant 2017-GYHLW01037, and in part by the National Natural Science Foundation of China under Grant 91748122 and Grant U1637207.

ABSTRACT Continuum robots, often taking inspiration from biomimetics, are an exciting novel research field and have a great capability. New continuum robots can be inspired by biologies such as seahorses, pipefish, and pipehorses, which have both strong skeleton and great dexterity. In this paper, the main idea contained is how to effectively employ the square components, which aim to imitate the armor and to connect the square components with the ball pairs and soft surface. For displaying the dexterity features of the square continuum robot (SCR), both the bending and twisting capabilities were studied. Meanwhile, a comparison was also considered in order to validate and analyze the dexterity differences in the numerical model, skeleton prototype, and SCR. The static characters of the SCR were shown both numerically and experimentally so that the mechanical properties are clear. Then, impact experiments were carried out to demonstrate the cushion effect. In addition, the maximum grasping load was also determined to quantize the grasping capability. Finally, a robot system was developed to handle objects with various shapes. Our results reveal that the SCR connected by the soft surface has improved flexibility, cushion stability, and better-grasping capability, with some loss of dexterity compared to SCR's skeleton.

INDEX TERMS Square continuum robot, bionic soft robotics, dexterity control, grasping capability.

I. INTRODUCTION

Unlike traditional rigid-link robots, continuum robots do not have any joints but instead possess a continuous backbone connected by flexible components [1]. Conventionally, robots composed of rigid links and joints, perform fast with precision and strength in assembly lines, but often with limited adaptability and safety concerns [2], [3]. Depending on the composition of (super-)elastic, soft material or a combination, continuum robots can be highly compliant, which provides an opportunity to remedy safety concerns [4]. They can be actuated to conform to various shapes so that it allows the robots to be used in multiple tasks, such as collapsed building rescue [5] or minimally invasive surgery [6], [7]. Continuum robots can also be actuated to achieve some numbers of the novel forms of functions if their attitudes are adjusted to encase and clench the objects.

In this type of application called prehension or grasp, robots are usually completely made of soft materials and primarily inspired by biological features such as elephant truck, octopus and snake [8]–[10]. Animal's softness and body compliance are salient features often exploited by biological systems to seek simplicity and to show reduced complexity in their interactions with the environment [11]–[13]. Therefore, these bio-inspired methods tend to be used to improve the grasping effect and shorten the manipulator time [14]. However, high compliance and comparably low structural stiffness also cause some problems. Due to stiffness limitation of soft materials like silicone or rubber, small interaction force can lead to large deformation of the robot itself. For these reasons, soft robot cannot be applied in dynamic capture conditions such as space debris collection where the debris sometimes spins [15]. It is possible for the continuum robot

The associate editor coordinating the review of this manuscript and approving it for publication was Yingxiang Liu.

FIGURE 1. Square-shaped tail fish. (a) Seahorse [16]. (b) Pipefish [17].

combining both soft and rigid materials to resolve the contradiction between the structural stiffness and shape adaption capability. However, continuum robots with a continuous backbone are mainly used for tip manipulations and are rarely applied for grasping nowadays. The reason is that it is hard to control force when rigid backbone touches hard objects and the contact area (the disk) like the tendon-driven robot presented in [18], [19] disperses in length direction. Herein, there remains an opportunity to develop a continuum robot with superior grasping capability.

Biology has always been a source of inspiration for engineers to make ever-more capable machines [20]. The fish armored with a square bony skeleton such as a seahorse, pipefish, or pipehorse (Fig.1) might give a new inspiration for continuum robot [21], [22] because of their high dexterity during grasping objects. The unique skeletons are arranged into several ring-like segments composed of four L-shaped bony plates surrounding a central vertebra [23]. Muscles attached to the vertebra transmit forces to the bony plates to control motion [24], [25]. In addition, recent studies have confirmed that the square skeleton is stronger than circular ones in the same scale [26]. Although these literatures show the controllable and strength advantages of the skeleton in robot application, the researches still focus on the biological mechanism [27]. So far, most of the proposed prototypes use 3D reconstruction to confirm the actual function of the biological features [28]–[30]. However, there are still some difficulties in biological tissue fabrication so that the existing reconstructed model is always complex and unstable. Therefore, this paper intends to redesign the structure to make it more simple, stable and usable for continuum robot. It is evident that the robot would have its advantages. Comparing to the continuum robot with backbone used for tip control [18], [19], the robot can deform to adapt, which means the possibility to grasp sensitive objects. Due to the existence of the central vertebra, the adaptable deformation is within certain range so that the robot has better shape preserving ability compared to the complete soft one. Besides, the skeleton performs similar function to armor so that the robot will be stiffened as the motion is beyond the extreme dexterity.

The details discussed in this paper are as follows: Firstly, a biomimetic square continuum robot (SCR) based on the simplified biological square tail has been presented. In this

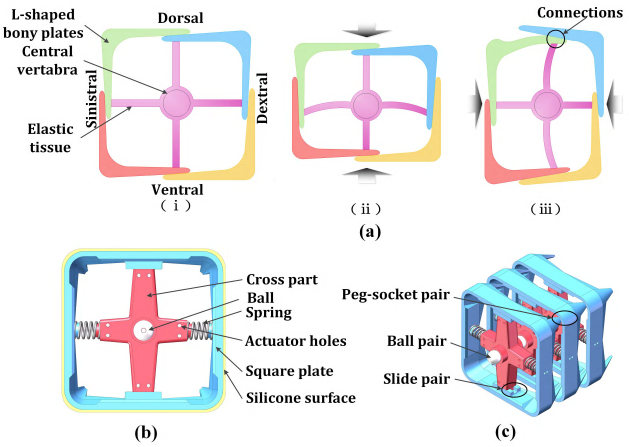

FIGURE 2. Bioinspired structure. (a) Biological characters of square-shaped fish's skeleton. A drawing based on [25]. (b) The component of square continuum robot (SCR). (c) Pairs in square continuum robot.

section, the structure and manufacturing methods of the robot are introduced. Secondly, the bending and twisting angles are analyzed in the numerical models and experiments to ensure the dexterity of SCR. The reasons for angle differences are discussed to identify the direction of the improvement. Thirdly, static properties of the SCR are shown in both numerical model and experiments for indicating mechanical characters. Then, compressing and impact experiments are implemented to demonstrate the cushion effect and the maximum grasping load is tested to quantize the grasping ability. After that, the robotic system is constructed to grasp objects with various shapes. Finally, the conclusion of the whole paper and the prospect of future work are listed.

II. STRUCTURE CHARACTER AND MANUFACTURING

A. BIOINSPIRED STRUCTURE

The design of this SCR inspired by square fish tails uses simplification and substitution methods. The armor of these fish can be divided into four L-shaped bony plates (Fig2a), whereas experiments indicate the existence of some pieces of evidence that certain connection takes effect between every nearby bony plate and restrains relative motion [25]. The experimental results in [25] has been redrawn in Fig.2a. As can be found from Fig.2a, the lateral L-plates termed a dextral-sinistral direction is harder to deform by comparing to a ventral-dorsal direction. Therefore, we use a whole square plate to mimic the armor. Meanwhile some soft joints are applied to permit buffer during the impact. These joints also constrain the degree of freedom (DOF) of mechanism and allow the armor slide only in one direction.

Besides the square plate, a component consists of one cross part and two springs as depicted by Fig.2b. As the effort of preserving the character of the buffer, the cross part which connects the spring in the slide direction should significantly be combined with the groove on the square plate that constitutes a slide pair (Fig.2c). Simultaneously, the actuator such as wire can only be arranged in the cross part in order to

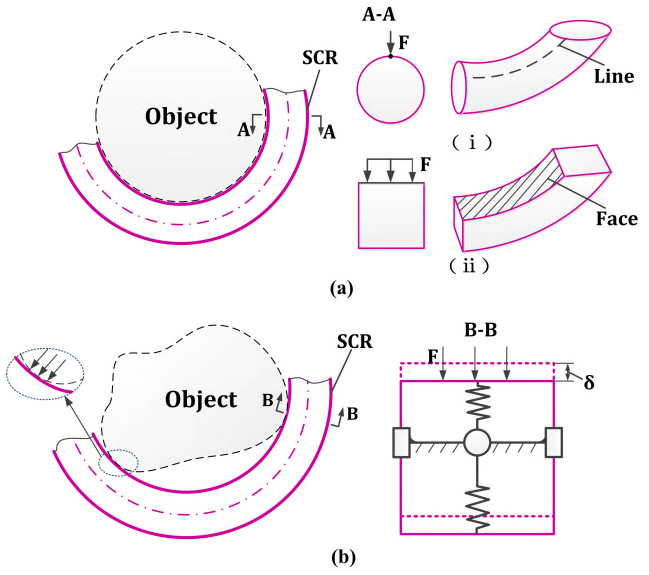

FIGURE 3. Grasping advantages of square continuum robot (SCR). (a) Larger interface in grasping regular objects. (b) Adaption capability in grasping irregular objects.

avoid any interference. Thus, there are actuator holes in the four directions of cross part mimicking the muscles as can be seen in Fig.2b. The SCR has more than 20 components to permit the robot for twisting 180 degrees (7 components are discussed here and one is considered as the base). Besides that, the connection between two components is ball pairs that resembles a vertebral column (Fig.2c). The peg-socket pair determines the maximum relative motion. As inspired by the groove in the biology [25], a socket has been improved. The parameters' effect of peg and socket to the bending and torsion properties will be discussed later. The structure introduced above mimics the skeleton of a square tail, so then the soft silicone surface is necessarily added. It is functioned as replication of a soft skin in these fishes to substitute the rods and springs in previous continuum robots [4], [5], [18], [19]. In another purpose, it is also used to endow the SCR a better recovery ability and apart the internal structure from the outside environment.

B. ADVANTAGE IN GRASPING

Although the simplification and substitution may inevitably cause some biological performance loss, the advantages of SCR in prehension are still apparent. As can be seen from Fig.3a that when the objects have regular shapes like a cylinder or cuboid, the SCR interface can be considered as a face while the circular continuum robots are nearly a line. As a result, by comparing to previous continuum robots with round appearance, the larger interface of SCR is safer so then it can increase the ultimate load to the sensitive objects. Besides, when the SCR is grasping irregular objects as depicted by Fig.3b, the soft joint composed of slide pairs and springs makes the square plate slide and the interface remain parallel at the same time. By means that the robot shows adaption ability to the irregular surface so that the interface enlarges.

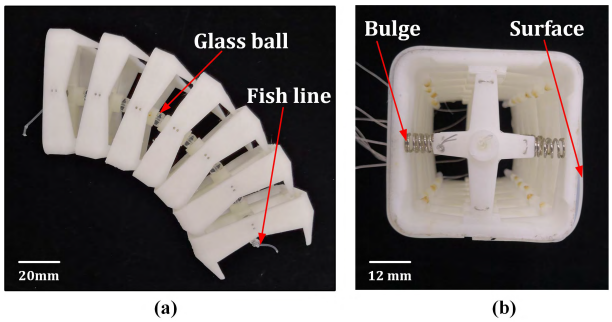

FIGURE 4. Prototype of square continuum robot (SCR). (a) Skeleton of SCR. (b) Cross section of SCR.

Obviously, the previous continuum robots made of a whole plate connected by springs or rods cannot achieve this adaption. Furthermore, unlike soft surface deformation driven by pneumatic, this kind of adaption has no effect on actuation because the actuator is arranged separately from the square plate. Moreover, the springs can also play as a buffer and absorb impact energy in the working condition that owns a certain relative velocity just like space debris collection [15].

C. MANUFACTURING METHODS

The development of 3D printing technology has made it possible to manufacture more efficient and cheaper prototype so that it can provide a good premise for bionics [31], [32]. Accordingly, the 3D printer (M200, Zortrax) was used to fabricate the square plate and cross part in this project. The ABS (Z-ABS, Zortrax) was used as the filament. Besides that, glass ball with a hole was also utilized in this case to reduce the friction in the ball pair (Fig.4a). The ball put in the special cross part owning a hemispherical groove and then the ball and cross part were tightened by a nylon fish line (1mm diameter) (Fig.4a). Figure.4b shows that the square plate and cross part have the bulges to assemble the springs.

The Silicone that has a similar character with skin is widely applied in the medical and bionic fields. Silicone surface surrounding to the SCR skeleton is made of a silicone board which has been cut into the same length of SCR skeleton and the same width of the square plate surface perimeter. The adhesion method is uniformly smearing glue on the single side of silicone and the adhesive side packages the square plates. Fortunately, the industrial production of the silicone board with adhesive surface is available (ZY450, Shenzhen Yongshunfa Plastics Materials, China). When it comes to assembly, SCR's skeleton should be fixed by a fixture to keep all of the square plates parallel before surface addition so that the influence of assembly error decreases. Then due to the bending of SCR which is mainly going to the direction of the spring arrangement (around y-axis) similar to the dorsal-ventral of square tail like the seahorse, the small gap should be disposed in the other direction as shown by Fig.5 in order to decrease the influence of assembly.

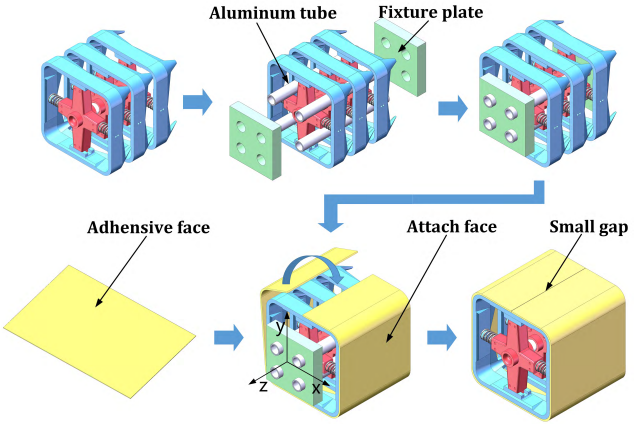

FIGURE 5. Methods for soft surface craftwork.

III. BENDING AND TORSION DEXTERITY ANALYSIS

It is clear that the ultimate bending and torsion angles limit the maximum curvature (κ) (Fig.6a) illustrates the dexterity and operation space. Therefore, it is necessary for further control and improvement to know which geometric parameter affects these results.

A. SKELETON BENDING AND TWISITING ANALYSIS

Due to the outstanding flexibility of the silicone, the surface influence was considered negligible here. Then, the free motion space of skeleton was substitute for SCR's dexterity. Referring to the biological features, the main factor that confines the relative motion of adjacent components is the peg-socket pair. So in this section, how this pair works is discussed firstly. It is obvious that the extreme deformation relates to the contact of peg and socket. As depicted in Fig.6a and Fig.6b, the contact point in twisting is a' and changes to b in bending. The dexterity can be calculated based on the angle of the peg (α) and the socket's geometric parameter. There is a slope in the socket angled β which satisfies $\beta < \alpha$ to ensure that peg and socket are only contacted in the edge of the next square plate as presented in Fig.6a. In SCR, the simplified model can be seen as some square pipe segments where the outside dimension is L, the internal dimension is I_s and the width is $w$that arranged into the same distance p. The socket on this pipe is mainly parameterized by the arc radius r_1, and edge length d. Edge length$d$that designed to avoid interface on the wing and expand the twisting is long enough. For further analysis, r_1 has the same circle center with the fillet and the radian is $\pi/2$ as depicted by Fig.6d.

Because of the socket, in pure bending the internal size of the pipe is changed into t as marked by the red dash line in Fig.6b, where $t \leq s$. The adjacent component rotates around the ball center O. The first component and the second one from the left side in Fig.6a are applied to clarify the position. According to the geometry, the maximum bending angle of two components is stated as follows:

$$\theta_b = \sin^{-1}\left(\frac{L\cos\alpha - p\sin\alpha}{2r}\right) - \alpha - \varphi \tag{1}$$

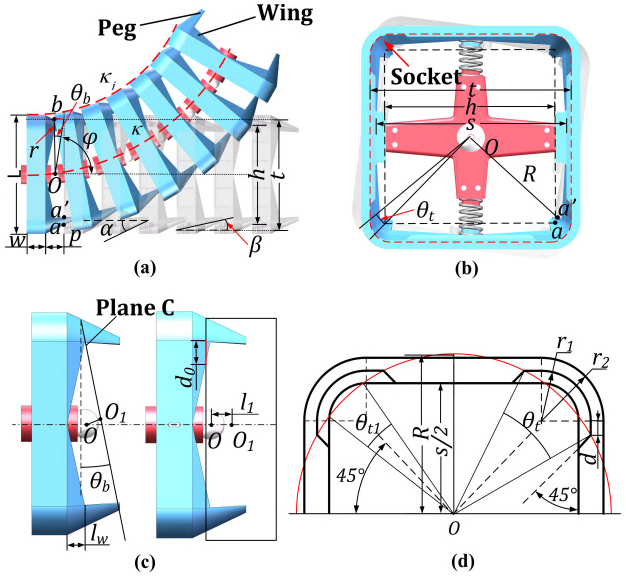

FIGURE 6. Bending and twisting analysis. (a) Skeleton bending. (b) Skeleton twisting. (c) 'd' analysis in bending situation. (d) Socket geometric analysis.

where the angle between the horizontal line and the second component φcan be written as $\varphi = \tan^{-1}(t/p)$. Besides that, the rotation radius of the square plate r can be written as $r = \sqrt{p^2 + t^2}/2$. Referring to equation (1), $\theta_b = f(\alpha, t, p, L)$. Here, we should calculate the edge length d to avoid the decrement of dexterity caused by wing which is designed to reinforce the peg as depicted in Fig.6a. The 3D views as shown by Fig.6c, indicate the calculation method that plane C coinciding with square plate lateral side that intercepts the wing to get the interference length d_0. Thus, it is obvious that $d \geq d_0$ and then d_0 can be written as:

$$d_0 = \frac{L - 2r_2}{2l_w}\left(l_w - \frac{p}{2} + \frac{t}{2}\cos(\varphi + \theta_b)\right) \tag{2}$$

where r_2 is the fillet radius (Fig.6d). Only the contact point on the wing does edge length of socket d affect and the relationship is

$$l_w \geq \frac{p}{2} + \frac{t}{2}\cos(\varphi + \theta_b) \tag{3}$$

As components rotate around the center point O, the motion trajectory of point a' in pure twisting is a circle as shown by Fig.6d. It is easy to get $\theta_t \geq \theta_{t1}$ where θ_t and θ_{t1} are the twisting angle with improved socket and the angle without improvement, respectively. Besides that, the situation that the motion trajectory of point a' crosses the arc portion of the socket is ignored to ensure the twisting angle is large enough. Hence, twisting angle θ_t depending on internal size t and peg distance h can be listed as follows:

$$\theta_t = 2\sin^{-1}\left(\frac{\sqrt{2}t}{2h}\right) - \frac{\pi}{2} \tag{4}$$

According to the structure, it is easy to get $h = L - 2p\tan\alpha$. Referring to equation (4), the range of edge length d can be

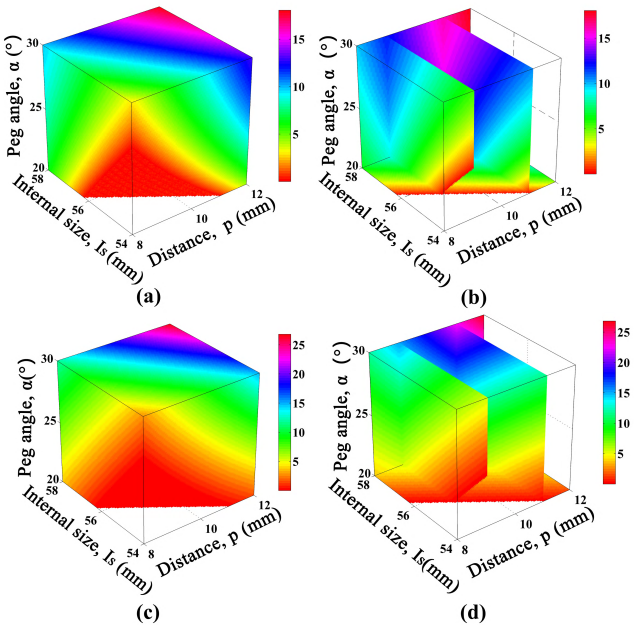

FIGURE 7. Geometrical parameters effect for bending and twisting angle. (a) Parameter 4D diagram of bending. (b) Internal slice of (a). (c) Parameter 4D diagram of torsion. (d) Internal slice of (c). The affecting parameters in two situations are distance, internal size and peg angle, and the fourth dimension is bending or twisting angle displaying by color.

calculated into

$$d \geq \frac{L}{2} - R\sin(\frac{\pi}{4} - \frac{\theta_t}{2}) - r_2 \tag{5}$$

where R is the twisting radius. In this project, the peg size is about 2mm which is much smaller than $\sqrt{2}\,h/2$. Herein, the size of the peg can be ignored and the twisting radius R can be expressed as $R = \sqrt{2}(L - 2p\tan\alpha)/2$.

In the analysis, the fundamental parameters have been selected as peg angle $\alpha = 25°, s = 54\text{mm}, p = 10.5\text{mm}, r_1 = 5.8\text{mm}, r_2 = 8\text{mm}$, external fillet $r_2 = 8\text{mm}$ in the scale of $L = 62\text{mm}$. All the parameters have been marked in Fig.6. Fillet related to the scale is designed to avoid stress concentration so that the size of fillet r_2 should be invariable. Due to the design of the socket, the actual effect shape can be seen as a pipe where internal size is I_s. It is easy to obtain$I_s = L - 2(r_2 - r_1) = t$. Hence, r_1 can be used to control the bending and twisting angle. According to equation (1) and (4), the segment distance p and peg angle α are also relative to dexterity. Above all, the dexterity based on these 3 variations has been plotted in 4D diagrams to ensure the tendency as illustrated by Fig.7. The parameter that does not satisfy boundary condition has already been removed. It can be found from Fig.7 that square plate distance p, internal size I_s and peg angle α are all positively correlated. As a result, enlarging value of these three parameters is quite useful to expand the dexterity. Furthermore, the extreme bending angle is mainly in 5∼15 degrees while twisting angle concentrates in the similar range, which may guide the selection of the component number for grasping. When the parameters selected above are substituted into equation (1) and (4), it can be acquired $\theta_B \approx 13.0°$ and $\theta_T \approx 12.5°$. Therefore, when SCR has n components, the total bending angle θ_B and total twisting angle θ_T are $(n-1)\theta_b$ and $(n-1)\theta_t$, respectively. In this topic, due to the component number is 7, it can be gained $\theta_B = 78.3°$ and $\theta_T = 75.3°$.

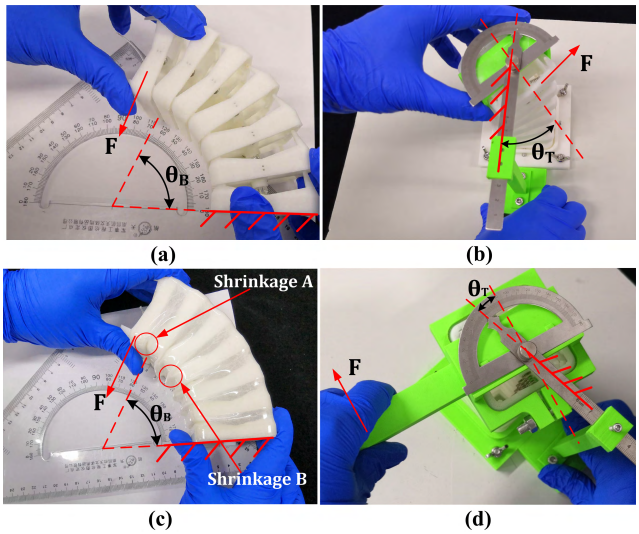

FIGURE 8. Bending and torsion angle tests. (a) Skeleton bending angle test. (b) Skeleton torsion angle test. (c) Bending angle test of square continuum robot (SCR). (d) Torsion angle test of SCR.

B. BENDING AND TORSION ANGLE TESTS

Before bending and torsion tests, prototype has been fabricated using the manufacturing methods above, and the parameter is as same as $\alpha = 25°, s = 54\text{mm}, p = 10.5\text{mm}, r_1 = 5.8\text{mm}, r_2 = 8\text{mm}$ in the scale of $L = 62\text{mm}$.

The skeleton without soft surface was tested for making a comparison with the numerical one. Ruler with protractor was applied to measure the skeleton bending angle during the tests (Fig.8a). The base (first square plate) was fixed in a horizontal line and the terminal part was moved to the final position when the motion meets big resistance (all square plates are contacting). Then mark the edge line of the terminal part and therefore the angle can be measured. We test ten times. After the biggest and smallest ones are removed, the average of the rest data is 78.0°.

A goniometer was used in the torsion angle test. SCR's skeleton, here, was fixed on the base and a fixture was introduced to locate the orientation (Fig.8b). The protractor in the goniometer can rotate with SCR, while the pointer keeps static. The torsion angle can be calculated by $\theta_T = |\theta_1' - \theta_2'|$. θ_1' is the angle that pointer directs in the right side and θ_2' is in the left side, where the original angle is 90°. Using the same data processing way as bending angle test, the torsion angle of SCR's skeleton is 82.5°. Bending and torsion angle were tested again, because of the application of silicone surface. Just as the measurement methods above, bending angle changes to 48.2° while twisting angle is 71.5°. Because of the large deformation force, the fixture of torsion angle test has been redesigned and the fixed force is enough in the base component (Fig.8d).

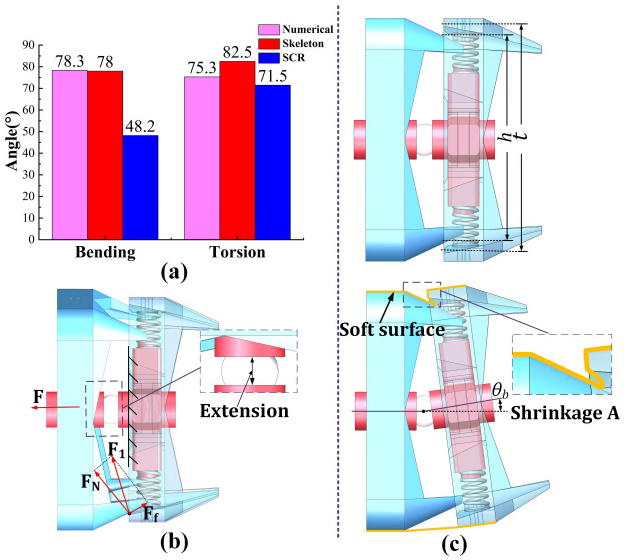

FIGURE 9. Dexterity comparison and discussion. (a) Angles in three situations. (b) Force analysis during twisting. (c) The effect mechanism of Shrinkage A.

C. DEXTERITY COMPARISON AND DISCUSSION

Next, the bending and torsion angle in three proposed situations (numerical, skeleton and SCR) were compared as depicted by Fig.9a.

Based on the numerical and experiment results as can be seen in Fig.9a, it has been found that the skeleton of SCR performs better dexterity in both bending and torsion tests. The bending angle of a skeleton is almost equal while the torsion angle is 9.56% larger compared to the numerical one. According to the force analysis as shown in Fig.9b, the resultant force is along the centerline during twisting so that the fish line extends and components distance p enlarges. Furthermore, just as equation (4), the augment of component distance can expand the twisting angle notably. It has been found as well that SCR strengthened by the surface has the near torsion angle than the skeleton that also gives evidence for skeleton torsion angle becoming larger. At the same time, the bending angle in SCR decreases sharply due to the irregular shrinkage direction. As can be seen from Fig.9c, the peg-socket pair is stuffed by silicone. Therefore, the shrinkage A enlarges the value of peg distance h and decreases the internal size t. Base on equation (1), it is easy to obtain the shrinkage causes the decrement of bending angle. Hence, there should be some improvements for the silicone surface in the future work in order to expand the dexterity of SCR.

IV. MECHANICAL CHARACTER OF SCR

The SCR, combing silicone surface, springs, and rigid parts, is rigid-flexible coupling. Besides owning great dexterity, the skeleton design endows SCR with both the contact stiffness and target shape adaption. Then, the addition of soft surface renders the robot to deform continuously and gives the self-recovery ability.

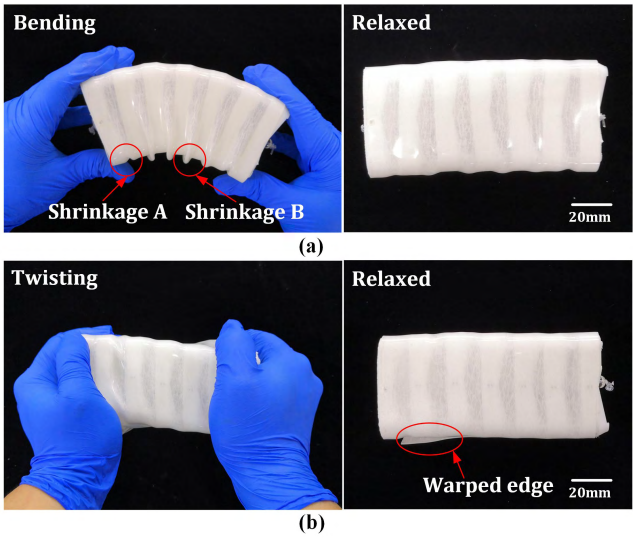

FIGURE 10. The recovery capability of square continuum robot (SCR). (a) SCR bending recovery test. (b) SCR torsion recovery test.

A. RECOVERY CHARACTER OF SCR

At this point, the SCR was tested with the silicone skeleton, which aims to ensure the recovery characteristics and dexterity of SCR. As can be seen in Fig.10, although there are some warp edges during twisting, SCR presents great shape memory capability in bending and twisting recovery tests compared to the skeleton owning a little recovery energy presented in Fig.4a. The surface in the ventral side will shrink as proposed above and according to the buckling direction, the shrinkage can be divided into Shrinkage A and Shrinkage B. Shrinkage A is pointed to SCR interior which has been suspected to affect the bending dexterity of SCR.

B. STATICS DEFORMATION RESPONSE

Although spring installed in SCR can give some recovery energy, it confines to the extreme large deformation. Furthermore, it is negligible in twisting because a whole square plate has been applied. The SCR without contact situation which has enough dexterity to grasp is the only one discussed in this paper. Due to the manufacturing method, the silicone surface adheres to the SCR skeleton. Herein, it is regarded the adhesion area has enough adhesive force so that skin can't slide on the surface of the square plate. And because of the use of the smooth glass ball, the friction in the ball pair can be neglected.

Although SCR has a similar function to the conventional soft robots, the analysis of the soft surface is quite different. Unlike conventional soft robot, due to mimic fish's square tail, SCR's components connected by the ball pair will restrict square plate to rotate around the center. Thus, what makes difference is that SCR's ventral side will shrink in bending while the surface of traditional soft robots always extends. Notice that as depicted by Fig.11a, the side closer to the bending center is called ventral side and the one away from the center is called dorsal side. For calculation, due to the

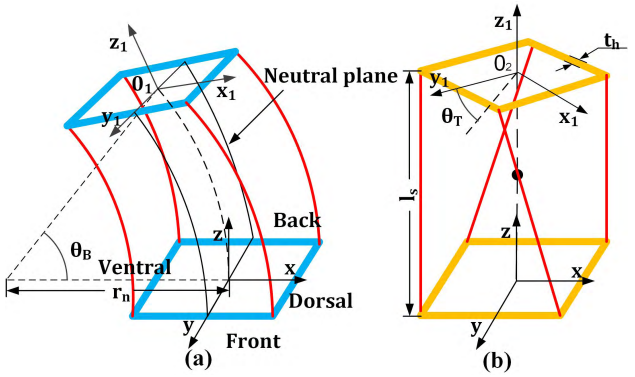

FIGURE 11. Simplified model of square continuum robot (SCR). (a) Bending deformation model. (b) Torsion deformation model.

distance between two components and their width is quite small, it has been regarded that the shape of SCR is functioned as a continuous curve. Just as a beam bending, there is a plane called neutral plane, of which length keeps constant during bending. It is apparent that the surface in the half part nearby ventral side will shrink, whereas the dorsal half will extend.

B Based on the hypothesis above, bending moment M_b, can be written as:

$$M_b = M_v + M_d \tag{6}$$

Here, M_v is ventral half side moment and M_d is the moment in the dorsal half side. The centerline of SCR has same curvature ρ and the valid length of the centerline (l_c) here is apparently $(n-1)(p+w)$. Where, n is the number of component in SCR which is set to be 7 so

$$r_n = \frac{1}{\rho} = \frac{(n-1)(p+w)}{\theta_B} \tag{7}$$

where r_n is the curvature radius of the center line (Fig.11a). So the surface length in the dorsal side can be written as follows:

$$l_d = \left(r_n + \frac{L+t_h}{2}\right)\theta_B \tag{8}$$

where t_h is the thickness of the silicone surface. According to the deformation and integral principle, M_d can be calculated as follows:

$$M_d = \frac{(l_v - l_c)\,(L+t_h)^2\, t_h E}{l_c} + M_1 \tag{9}$$

Notice that the length of the real extended silicone is $l_c/2$ because the surface is sticking on the square part. E is the Young modulus of the silicone applied on the surface. Shore A of silicone surface is 75 so that the corresponding $E = 3.6$MPa. Based on cutting the surface into a small bar, the front-back side moment in the ventral half M_1 (Fig.11a) can be written as follows:

$$\begin{aligned} M_1 &= \frac{4Et_h}{l_c}\int_0^{L/2}((r_n+x)\theta_B - l_c)x dx \\ &= \frac{Et_hL^2}{6l_c}(3r_n\theta_B + L\theta_B - 3l_c) \end{aligned} \tag{10}$$

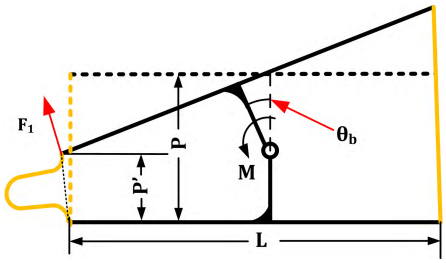

FIGURE 12. Shrinkage analysis diagram.

The shrinkage recovery moment M_v is made of a moment in the ventral half. The shrinkage shape between two square plates is relative to component distance after bending p' as illustrated by Fig.12.

$$p' = \frac{p}{2}(1+\cos\theta_b) - \frac{L}{2}\sin\theta_b \tag{11}$$

At this point, the shrinking process can be regarded as a plate stability problem. The deformation of silicone surface will change from linear situation into a buckling one. The calculation of the recovery force after buckling is quite complex but most of the materials have the same character where the recovery force is a little smaller than the critical load after buckling. So the recovery force F_1 is substituted with the critical force F_{cr}.

$$F_{cr} = k_c\frac{\pi^2 t_h^3 E}{12(1-\mu^2)(L+t_h)} \tag{12}$$

where the critical load coefficient k_c can be written as follows:

$$k_c = \left(\frac{mL+mt_h}{p} + n^2\frac{p}{mL+mt_h}\right)^2 \tag{13}$$

Based on the experiment result shown by Fig.10, $m = 1$ and $n = 0$are the order in the p and L direction, respectively. So, it is easy to get$k_c = 39.7$. Then by substitution k_c into equation (12), it can be acquired $F_{cr} \approx 1.71$N which is the ideal critical load. Therefore, it is apparent that the deformation before buckling is

$$\frac{p-\delta}{p} = \frac{F_{cr}}{Et_h(L+t_h)} \tag{14}$$

where $\delta = p'/\cos\theta_b$. And according to equation (14), the buckling will happen in a very small bending angle. F_{cr} is substituted as the react force caused by shrinkage. Thus

$$M_v = \frac{3}{4}(n-1)(L+t_h)F_{cr} \tag{15}$$

Then, by substituting all the condition into equation (6), SCR ideal bending angle-force relationship can be acquired as shown in Fig.13c. The reason behind the transition in Fig.13c is that the buckling occurs in this position and the critical force is simply substituted into the force after buckling. Unlike rotating around the ball center in bending, SCR has only one rotating center in twisting. SCR can be simplified into a silicone square pipe neglecting the attached area to the

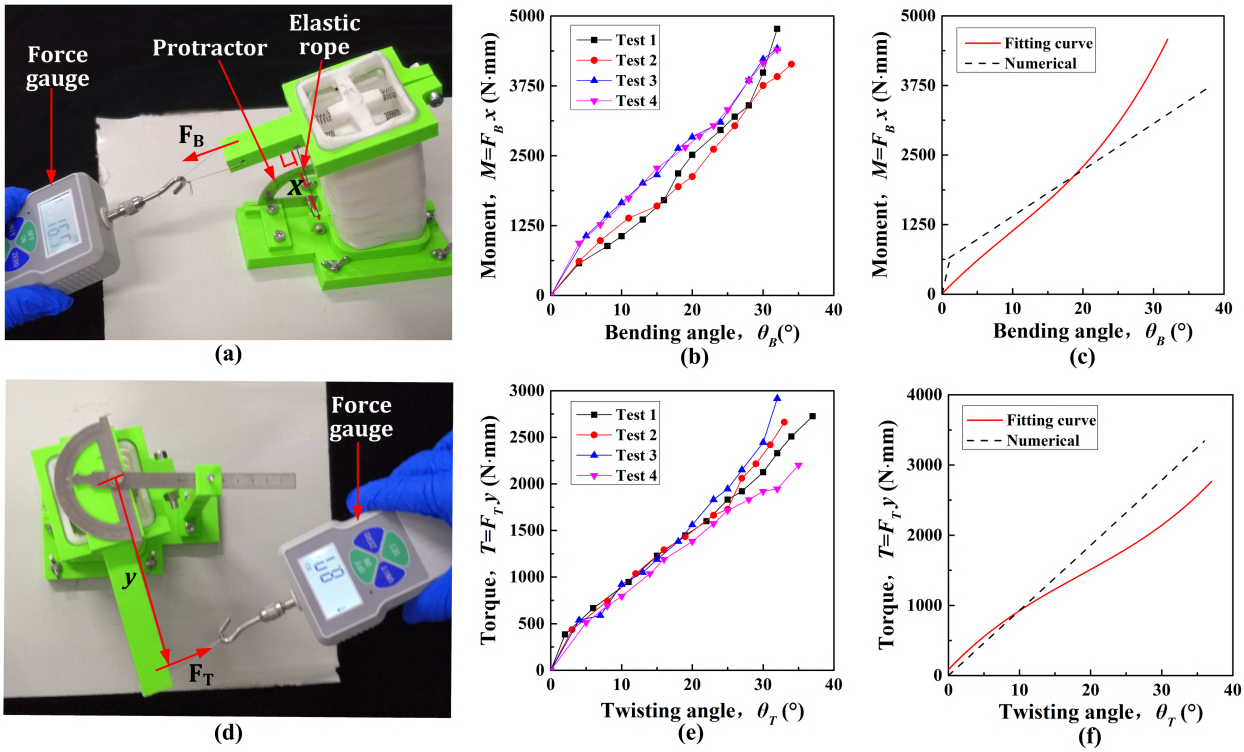

FIGURE 13. Deformation response of square continuum robot (SCR). (a) Test method of bending deformation response: Force gauge pulls SCR fixed on the base. (b) Curves of bending deformation response data. Single curve is tested in one continuous deformation. (c) Numerical curve of bending response calculated by the simplified mathematic model and fitting curve based on the experiment data. (d) Test methods of twisting deformation response: Force gauge pulls the force arm in the frock. (e) Twisting deformation curves. Single curve is tested in one continuous deformation. (f) Numerical curve of twisting response calculated by the simplified mathematic model and fitting curve based on the experiment data.

square plate where thickness is donated by t_h and the twisting equivalent length l_s is$(n-1)p$ as can be seen in Fig.11b. Thus, the shell beam model used to express the twisting situation can be expressed as follows:

$$T = \frac{4GA^2 t_h \theta_T}{l_s \sum l_i} \tag{16}$$

In equation (16), $G = E/2(1+\mu)$ is the shear modulus made of Young modulus E, and Poisson's ratio μ. The Poisson's ratio of silicone surface used in this project is about 0.48. So it can been gained that $G = 1.22$MPa. Where $\sum l_i$ presents the perimeter of cross section midline and $\sum l_i = \pi(2r_2 + t_h) + 4(L-2r_2-t_h)$ in SCR. Furthermore, A is the encircled area of cross section midline and$A = (L+t_h)^2+(\pi-4)(r_2+0.5t_h)^2$. Above all, the numerical curves based on the numerical calculation are plotted in Fig.13f.

For clarifying statics character, the relationship of the SCR's moment-angle and torque-angle were tested. In bending tests, the bending angle θ_B can be measured by the angle that elastic rope points (Fig.13a). Then, based on the bending angle and equation (11), the force arm x can be obtained. The force corresponding to the deformation remains parallel to the handle and it can be read directly with the force gauge. Therefore, the moment that held up by SCR during deformation process can be acquired. The SCR has been tested four times and the test data is listed in Fig.13b. The result indicates a similar magnitude and same trend that the angle-moment curve is positively correlated. SCR seems to have fixed stiffness as shown in Fig.13b. According to Fig.13c, the test data was fitting by a cubic function. Obviously, there is an intersection point between the numerical curve and fitting curve (Fig.13c). The reason is that single shrinkage of soft surface contacts because of surface thickness and large deformation.

Referring to twisting tests, a series of fixtures that similar to the dexterity tests were used to measure the angle where the actuation force was applied by the force gauge. The force gauge remained to be vertical to the force arm where the length was y. Therefore, it is easy to get the torque applied to SCR that can be obtained by applying $T = F_T y$ as depicted in Fig.13d. In this project, the performance was tested four times as shown in Fig.13e. The fitting process of the data was done by a cubic function. Unlike the bending test, fitting curve fits good at the beginning of deformation compared to the numerical curve and then the value becomes smaller than the numerical one as can been seen from Fig.13f. The numerical model considers the ideal situation that there is enough adhesive force between the surface and square plate, whereas the curved surface in Fig.10 shows some area warps. The warped edge in the deformation has a meaning that some portion of surfaces are invalid and offers less recovery force compared to the ideal situation.

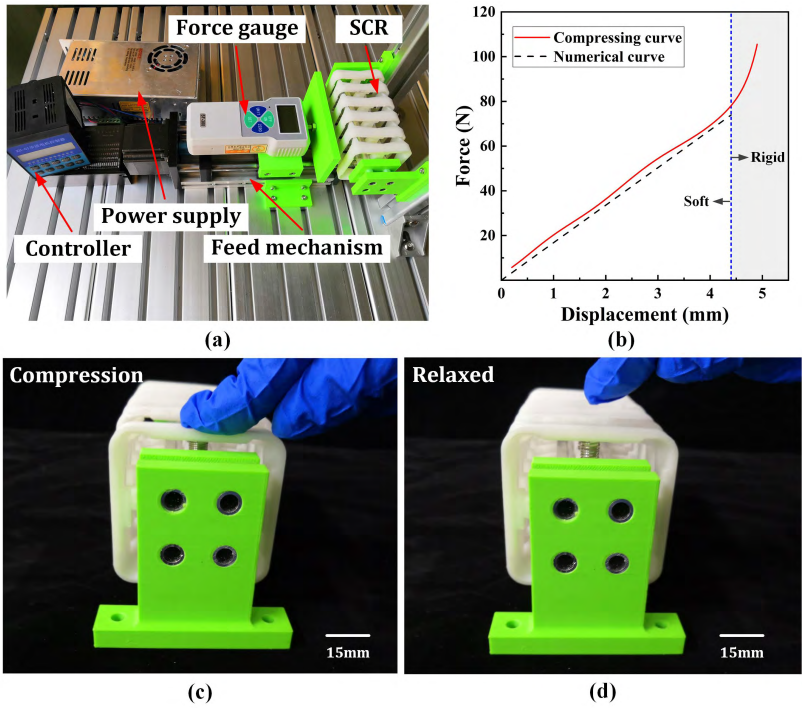

FIGURE 14. Stiffness and stability of square continuum robot (SCR). (a) Stiffness tests device. Test method is that controller controls feed mechanism connected with force gauge to compress SCR and the displacement is calculated by pulse number given to step motor. (b) The force displacement curve both in numerical and experiment. (c) SCR in compressing. (d) SCR after compressing.

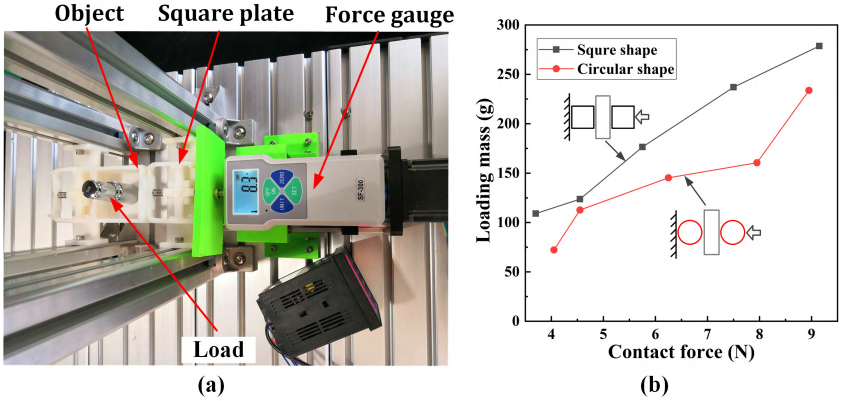

FIGURE 15. Grasping capability comparison. (a) Grasping capability experiment device. The test method is that load the robot components in both square and circular shape by pushing plate connected by force gauge and add weight on the object to obtain the extreme gripping force. The contact force can be read in the force gauge. (b) Contact force and the extreme loading mass curve.

C. COMPRESSING AND IMPACT EXPERIMENTS

Soft joints mounted on every square component endow the SCR to have an adaption capability and to function as a cushion when impact occurs in the dynamic grasping like a space debris capture. So it is necessary to explore the contact stiffness and impact stability of SCR. Spring plays the soft roles in a square component, thus the stiffness can be easily calculated as follow:

$$K_s = n\frac{Gd^4}{4ND^3} \tag{17}$$

where, n is the number of square components, G is the shear modulus of the spring material, d is the spring wire diameter, $D$is the pitch diameter, and N is the spring valid cylinder number. There are two springs in a square component. The geometry parameter has been substituted into equation (17), and $K_s = 16.8N/\text{mm}$ is acquired. The friction can be ignored due to the slide pair has been polished before assembly. The compressing experiment has been done by fixing the cross part where the actuators arranged as presented by Fig.14a. Both the numerical and experimental results were plotted in Fig.14b. For protecting the actuators in cross part,

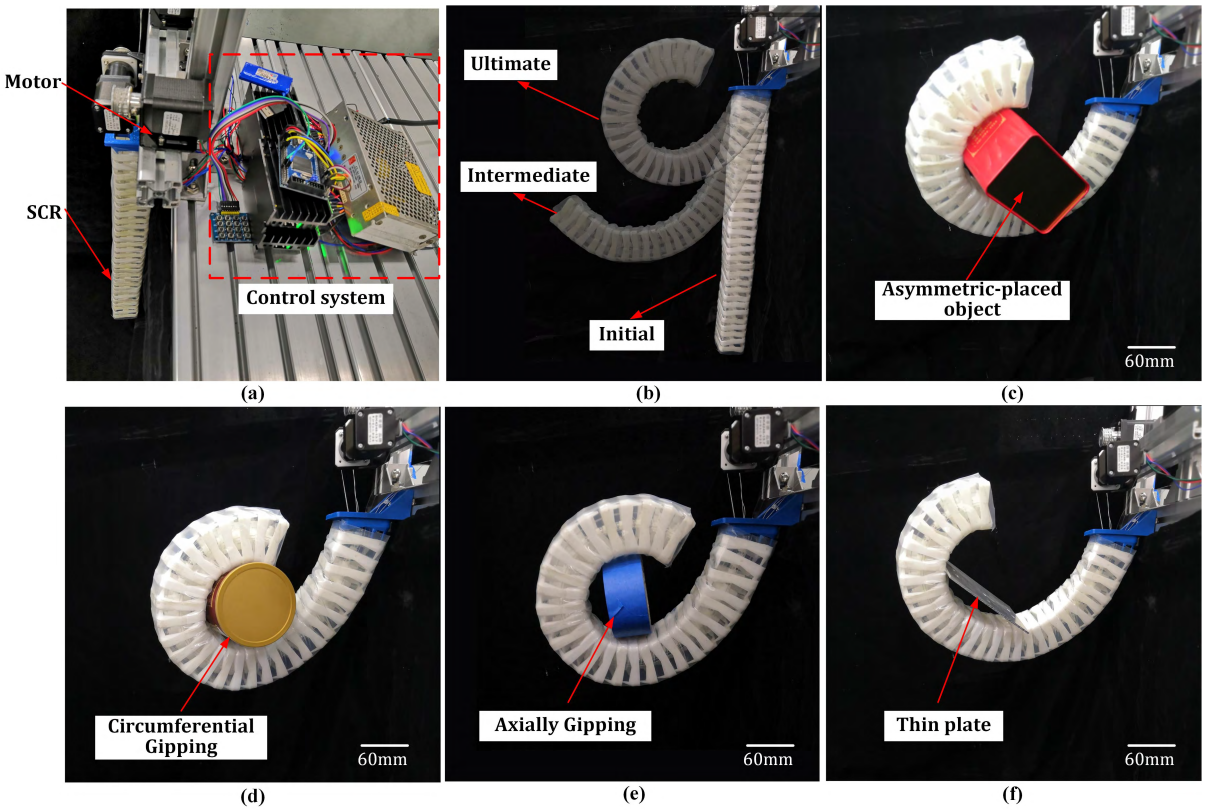

FIGURE 16. Robot system configuration and grasping demonstration to show the capabilities of handling different shape of objects. (a) The robot system configuration of SCR. (b) The motion demonstration of SCR, displaying the initial, intermedia and ultimate state of SCR. (c) Gripping an asymmetrical cubic object. (d) and (e) Gripping a cylindrical objects in different directions. (f) Gripping an aluminum plate.

the spring length is limited so that the stiffness transition is obviously near the maximum compressing displacement of spring, $L_D = L_s - (N + 3)d$. Where L_s is the original length of spring and $N + 3$ is the total circle number. Therefore, compressing process can be divided into two parts called the soft and rigid part respectively. Besides more chances to contact the object and to perform better-grasping effect, the softness of SCR makes a rigid surface can be applied in sensitive targets, while the rigidity supplies enough a grasping force without interfering actuators. For clarifying the impact protection capability, it has been tried to compress and hammer the robot (Here, the skeleton is the only one used for this observation). The compressing process is shown as the movie S1, while Fig.14d displays the result after compressing. Moreover, hammering experiments are shown in the appendix movie S2. It is apparent that SCR owns excellent shape retention and can remain square shape during big deformation or impact.

V. GRASPING EXPERIMENTS

A. GRASPING FORCE EXPERIMENT

Some advantages of SCR's grasping ability have been illustrated in section II. Here, for displaying the improvement visually, the simplified grasping experiments have been done. The test method was to load the object between two components by adding the weight to evaluate grasping force. In this method shown by Fig.15a, the variation of shape manipulation and actuation force difference can be ignored. Due to the principle of the internal force balance, contact force applied to the robot can be quantized by force gauge. The components in the same scale and manufacturing way with different shapes have been used in the experiments. It has been tested five times in the same contact force and then accordingly the average of the loading mass was obtained. The result has been plotted in Figure.15b. Based on these results, It can be found that the square components from SCR withstands a larger extreme load than the circular ones. Therefore, it can be concluded that SCR owns better-grasping ability.

B. GRASPING DEMOSTRATION

As can be seen from all the content presented above, the characters of SCR has been discussed. In this topic, the robot system with this special square structure was established. But the soft surface is thinner than the previous one in purpose of driving and expanding the dexterity. As depicted in Fig.16a that the system consists of a continuum robot arm, actuators, and control system. There are 30 square components to form a 0.6 meters long robot arm with the same structure as presented above. The actuation method is still cable-driven with four motors now. A Single Chip Microcomputer (STM32 F103ZET6) connected with the

keyboard as a controller is used in this project. Because of the high dexterity of SCR, the robot can deform to various attitudes. Here, three different attitudes illustrated by Fig.16b present initial, intermedia and ultimate configuration respectively. Then, SCR was used to grasp some objects with various shapes.

Due to the large interface and structural characters, SCR can grip the objects in asymmetric placement condition so that it can simplify the location and manipulation. As can be seen from Fig.16c that the robot can successfully lift the cubic jar that was placed asymmetrically. And it is difficult for the robot with a circular shape to offset the biasing moment caused by gravity. The robot can also handle the cylindrical objects but what makes a difference is whether the interface is along circles or vertical to circle are both fine as seen from Fig.16d, Fig.16e. It is evident that it is hard for a circular robot to hold weight when the situation is line-to-line contact. Fig.16f illustrates the outstanding capability of a soft-rigid coupling mechanism to bear the stress concentration. For grasping plate-like objects, a small load may cause large deformation for soft materials and affects or even breaks the soft body.

VI. CONCLUSION

This paper focuses on the development of a continuum robot to be applied in grasping objects by shape envelopment in which the soft joints of the robot may enhance adaption and absorb impact energy. A square continuum robot (SCR) configuration inspired by fish owning square tail was proposed. The dexterity about free bending and torsion capabilities of the SCR model were analyzed and statics response was shown. Based on the numerical model and experiments result, it is concluded that the effect factors introduced in the numerical model have the same positive correlation to the bending or torsion angle, which gives guidance for SCR design. The angle comparison of numerical model, skeleton, and SCR shows the uncertain direction of shrinkage caused by soft surface deformation is the main reason for dexterity difference in these situations. The statics response indicates that soft surface endows SCR great recovery capability and necessary deformation transmission ability. For displaying the advantages of SCR, the impact experiment indicates SCR with a simple structure has stable adaption ability while the grasping force experiment shows SCR has better grasping capability than the circular ones in the same condition. Finally, based on the work above, the robot system was established and the robot was controlled to grasp various objects challenging for conventional robots. In subsequent work, there will be an improvement in the silicone surface to avoid the crinkle of silicone surface interfering motion during bending. Besides that, the vision system will also be introduced to discover objects and control the attitude. Hopefully, SCR can achieve dynamic capture in the future.

ACKNOWLEDGMENT

(Long Li and Tao Jin contributed equally to this work.)

REFERENCES

[1] B. A. Jones and I. D. Walker, "Kinematics for multisection continuum robots," *IEEE Trans. Robot.*, vol. 22, no. 1, pp. 43–55, Feb. 2006.

[2] S. Kim, C. Laschi, and B. Trimmer, "Soft robotics: A bioinspired evolution in robotics," *Trends Biotechnol., Rev.*, vol. 31, no. 5, pp. 23–30, May 2013.

[3] C. Q. Xiang, J. L. Guo, Y. Chen, L. N. Hao, and S. Davis, "Development of a SMA-fishing-line-McKibben bending actuator," *IEEE Access*, vol. 6, pp. 27183–27189, 2018.

[4] M. Langer, E. Amanov, and J. Burgner-Kahrs, "Stiffening sheaths for continuum robots," *Soft Robot.*, vol. 5, no. 3, pp. 291–303, Jun. 2018.

[5] R. J. Webster, III, and B. A. Jones, "Design and kinematic modeling of constant curvature continuum robots: A review," *Int. J. Robot. Res.*, vol. 29, no. 13, pp. 1661–1683, 2010.

[6] Z. Li, H. Ren, P. W. Y. Chiu, R. Du, and H. Yu, "A novel constrained wire-driven flexible mechanism and its kinematic analysis," *Mech. Mach. Theory*, vol. 95, pp. 59–75, Jan. 2016.

[7] J. Burgner-Kahrs, D. C. Rucker, and H. Choset, "Continuum robots for medical applications: A survey," *IEEE Trans. Robot.*, vol. 31, no. 6, pp. 1261–1280, Dec. 2015.

[8] C. Laschi, M. Cianchetti, B. Mazzolai, L. Margheri, M. Follador, and P. Dario, "Soft robot arm inspired by the octopus," *Adv. Robot.*, vol. 26, no. 7, pp. 709–727, 2012.

[9] G. J. Bao *et al.*, "Pneumatic bio-soft robot module: Structure, elongation and experiment," *Int. J. Agricult. Biol. Eng.*, vol. 10, no. 2, pp. 114–122, Mar. 2017.

[10] C. Laschi, B. Mazzolai, and M. Cianchetti, "Soft robotics: Technologies and systems pushing the boundaries of robot abilities," *Sci. Robot., Rev.*, vol. 1, no. 1, p. 11, Dec. 2016, Art. no. UNSP eaah3690.

[11] T. G. Thuruthel, Y. Ansari, E. Falotico, and C. Laschi, "Control strategies for soft robotic manipulators: A survey," *Soft Robot.*, vol. 5, no. 2, pp. 149–163, Apr. 2018.

[12] R. F. Shepherd *et al.*, "Multigait soft robot," *Proc. Nat. Acad. Sci. USA*, vol. 108, no. 51, pp. 20400–20403, 2011.

[13] F. Iida and C. Laschi, "Soft robotics: Challenges and perspectives," *Procedia Comput. Sci.*, vol. 7, no. 29, pp. 99–102, 2011.

[14] A. Al-Ibadi, S. Nefti-Meziani, and S. Davis, "Active soft end effectors for efficient grasping and safe handling," *IEEE Access*, vol. 6, pp. 23591–23601, 2018.

[15] M. H. Shan, J. Guo, and E. Gill, "Review and comparison of active space debris capturing and removal methods," *Prog. Aerosp. Sci.*, vol. 80, pp. 18–32, Jan. 2016.

[16] SEAHORSE. (2018). *Coral Key Scuba and Travel*. Accessed: Feb. 20, 2019. [Online]. Available: https://www.coralkeyscuba.com/blog/2018/6/11/ogll87zzzgl2y7vzllntavxu6ste2m

[17] Beady Pipefish, Hippichthys Penicillus. (2010). *Hippichthys in Fishes of Australia*. Accessed: Feb. 20, 2019. [Online]. Available: http://fishesofaustralia.net.au/home/genus/673

[18] K. Xu, J. Zhao, and M. Fu, "Development of the SJTU unfoldable robotic system (SURS) for single port laparoscopy," *IEEE/ASME Trans. Mechatronics*, vol. 20, no. 5, pp. 2133–2145, Oct. 2015.

[19] M. Mahvash and P. E. Dupont, "Stiffness control of surgical continuum manipulators," *IEEE Trans. Robot.*, vol. 27, no. 2, pp. 334–345, Apr. 2011.

[20] D. Rus and M. T. Tolley, "Design, fabrication and control of soft robots," *Nature*, vol. 521, pp. 467–475, May 2015.

[21] M. E. Hale, "Functional morphology of ventral tail bending and prehensile abilities of the seahorse, *Hippocampus Kuda*," *J. Morphol.*, vol. 227, no. 1, pp. 51–65, Jan. 1996.

[22] K. Kumaravel, E. R. Priya, S. Ravichandran, and T. Balasubramanian, "Morphological perspectives of the seahorse Hippocampus Kuda (Bleeler) vertebral system," *E-Int. Sci. Res. J.*, vol. 2, no. 1, pp. 63–69, 2010.

[23] T. Praet, D. Adriaens, S. Van Cauter, B. Masschaele, M. De Beule, and B. Verhegghe, "Inspiration from nature: Dynamic modelling of the musculoskeletal structure of the seahorse tail," *Int. J. Numer. Methods Biomed. Eng.*, vol. 28, no. 10, pp. 1028–1042, Oct. 2012.

[24] C. Neutens *et al.*, "Grasping convergent evolution in syngnathids: A unique tale of tails," *J. Anatomy*, vol. 224, no. 6, pp. 710–723, Jun. 2014.

[25] M. M. Porter, E. Novitskaya, A. B. Castro-Ceseña, M. A. Meyers, and J. McKittrick, "Highly deformable bones: Unusual deformation mechanisms of seahorse armor," *Acta Biomaterialia*, vol. 9, no. 6, pp. 6763–6770, Jun. 2013.

[26] M. M. Porter, D. Adriaens, R. L. Hatton, M. A. Meyers, and J. McKittrick, "Why the seahorse tail is square," *Science*, vol. 349, no. 6243, Jul. 2015, Art. no. aaa6683.

[27] M. M. Porter and N. Ravikumar, "3D-printing a 'family' of biomimetic models to explain armored grasping syngnathid fishes," *Bioinspiration, Biomimetics*, vol. 12, no. 6, Dec. 2017, Art. no. 066007.
[28] B. E. Flammang and M. E. Porter, "Bioinspiration: Applying mechanical design to experimental biology," *Integr. Comparative Biol.*, vol. 51, no. 1, pp. 128–132, Jul. 2011.
[29] A. J. Ijspeert, "Biorobotics: Using robots to emulate and investigate agile locomotion," *Science*, vol. 346, no. 6206, pp. 196–203, 2014.
[30] S. V. Cauter *et al.*, "Design from nature: Kinematic modeling of the seahorse tail," in *Proc. SIMULIA Customer Conf. (SCC)*, 2010, pp. 385–386.
[31] N. W. Bartlett *et al.*, "A 3D-printed, functionally graded soft robot powered by combustion," *Science*, vol. 349, no. 6244, pp. 161–165 2015.
[32] M. M. Porter, N. Ravikumar, F. Barthelat, and R. Martini, "3D-printing and mechanics of bio-inspired articulated and multi-material structures," *J. Mech. Behav. Biomed. Mater.*, vol. 73, pp. 114–126, Sep. 2017.

LONG LI received the Ph.D. degree in mechanical design and theory from the Harbin Institute of Technology (HIT), Harbin, China, in 2013.

His research interests include mobile robots, bionic robots, soft robots, and multi-robot systems. He is a member of the Lab of Intelligent Mechanism and Advanced Robot (LIMAR) Research Team.

TAO JIN received the B.Eng. degree in mechanical design manufacturing and automation from Zhejiang Sci-Tech University, Hangzhou, China, in 2017. He is currently pursuing the M.S. degree with the School of Mechatronic Engineering and Automation, Shanghai University.

His research interests include bionic robots, soft robots, and robotic sensing. He is a member of the Lab of the Intelligent Mechanism and Advanced Robot (LIMAR) Research Team.

YINGZHONG TIAN received the Ph.D. degree in mechanical manufacture and automation from Shanghai University, Shanghai, China, in 2007, where he is currently the Director of research with the Lab of Intelligent Mechanism and Advanced Robot (LIMAR) Research Team.

His research interests include mobile robots, bionic robots, multi-robot systems, and image processing.

FEI YANG was born in 1985. He received the Ph.D. degree from the Harbin Institute of Technology, Harbin, China, in 2014, where he is currently an Associate Professor with the Research Center of Aerospace Mechanism and Control.

His main research interests include bionic robots, connection, and separation mechanism in space.

FENGFENG (JEFF) XI received the B.S. degree in manufacturing engineering and the M.S. degree in precision machining from Shanghai University, China, in 1982 and 1984, respectively, and the Ph.D. degree in robotics and automation from the University of Toronto, Canada, in 1993.

In 1994, he joined the National Research Council of Canada (NRC) and progressed from an Assistant Research Officer to an Associate Research Officer and the Project Leader. He has been appointed as the a Distinguished Professor with the School of Mechatronic Engineering and Automation, Shanghai University, and with the Shanghai Key Laboratory of Intelligent Manufacturing and Robotics, since 2014. He is currently a Professor and the Director of Robotics and Intelligent Manufacturing Research Laboratory, Ryerson University, Canada. His research interests include robotics and mechanisms, manufacturing and automation, and inspection and condition monitoring.